Biochemistry
Article
Cite This: Biochemistry XXXX, XXX, XXX−XXX
pubs.acs.org/biochemistry

K-Ras^{G12D} Has a Potential Allosteric Small Molecule Binding Site

Huizhong Feng,[†] Yan Zhang,[‡] Pieter H. Bos,[†] Jennifer M. Chambers,[‡] Marcel M. Dupont,[†] and Brent R. Stockwell*[,†,‡]

[†]Department of Biological Sciences and [‡]Department of Chemistry, Columbia University, Northwest Corner Building, 12th Floor, MC 4846, 550 West 120th Street, New York, New York 10027, United States

Supporting Information

ABSTRACT: *KRAS* is the most commonly mutated oncogene in human cancer, with particularly high mutation frequencies in pancreatic cancers, colorectal cancers, and lung cancers [Ostrem, J. M., and Shokat, K. M. (2016) *Nat. Rev. Drug Discovery 15*, 771−785]. The high prevalence of *KRAS* mutations and its essential role in many cancers make it a potentially attractive drug target; however, it has been difficult to create small molecule inhibitors of mutant K-Ras proteins. Here, we identified a putative small molecule binding site on K-Ras^{G12D} using computational analyses of the protein structure and then used a combination of computational and biochemical approaches to discover small molecules that may bind to this pocket, which we have termed the P110 site, due to its adjacency to proline 110. We confirmed that one compound, named K-Ras allosteric ligand KAL-21404358, bound to K-Ras^{G12D}, as measured by microscale thermophoresis, a thermal shift assay, and nuclear magnetic resonance spectroscopy. KAL-21404358 did not bind to four mutants in the P110 site, supporting our hypothesis that KAL-21404358 binds to the P110 site of K-Ras^{G12D}. This compound impaired the interaction of K-Ras^{G12D} with B-Raf and disrupted the RAF-MEK-ERK and PI3K-AKT signaling pathways. We synthesized additional compounds, based on the KAL-21404358 scaffold with more potent binding and greater aqueous solubility. In summary, these findings suggest that the P110 site is a potential site for binding of small molecule allosteric inhibitors of K-Ras^{G12D}.

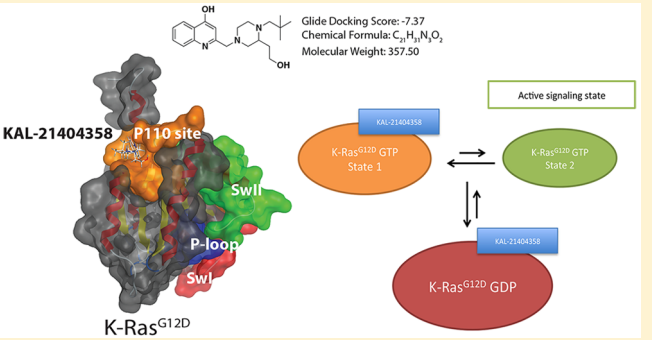

Ras proteins belong to the small GTPase family and are involved in transmitting growth, survival, and proliferation signals within cells. As a GTPase, Ras cycles between a GTP-bound state and a GDP-bound inactive state, the transition of which is regulated by guanine nucleotide exchange factors (GEFs) and GTPase-activating proteins (GAPs).[2] Two regions of Ras proteins, switch I (residues 30−40) and switch II (residues 60−76), undergo substantial conformational changes and form effector−protein interaction surfaces upon GTP binding.[3] In the GTP-bound active state, Ras interacts with effector proteins and activates downstream cellular signal transduction pathways, including the RAF-MEK-ERK, PI3K-AKT-mTOR, and RalGDS pathways.[4] Oncogenic mutants of Ras are locked in an active signaling state: the constitutive activation of Ras downstream signaling results in sustained proliferation, metabolic reprogramming, inhibition of apoptosis, and other hallmarks of cancer.[5]

There are three common RAS genes in humans: *KRAS*, *HRAS*, and *NRAS*. The frequencies and distribution of RAS gene mutations are not uniform among these three family members.[6] *KRAS* is the most frequently mutated gene and is altered in 86% of *RAS*-altered cancers. G12, G13, and Q61 are three hot spot point mutations found around the RAS GTP binding site. Among these mutations, G12D mutations are predominant in pancreatic ductal adenocarcinoma and colon and rectal carcinomas.[7] The high prevalence of *KRAS* mutations in cancers suggests it may be a potentially valuable drug target. However, there are still no effective inhibitors directly targeting K-Ras mutant proteins that are suitable for clinical use.

K-Ras is considered a challenging drug target for two main reasons. First, there does not seem to be a deep, hydrophobic pocket on the surface of K-Ras suitable for potent and selective small molecule binding; the only notable binding pocket on K-Ras is the nucleotide binding pocket, which binds GTP/GDP with picomolar affinity, making it an impractical target site for small molecule drugs.[8] Second, K-Ras, like roughly 85% of other human proteins, exerts its biological effects via protein−protein interactions, which are often difficult to disrupt with small molecules, due to their large surface areas and the diffuse nature of the interactions between them.[9] Despite these difficulties, direct K-Ras inhibitors have been explored using several strategies: (1) targeting G12C-specific K-Ras mutants with covalent, cysteine-reactive electrophilic inhibitors,[10−12] (2) blocking K-Ras−effector interactions by developing small molecule and peptide inhibitors,[13−15] (3) interrupting

Received: December 21, 2018
Revised: April 29, 2019
Published: May 1, 2019

DOI: 10.1021/acs.biochem.8b01300
Biochemistry XXXX, XXX, XXX−XXX

nucleotide exchange, including the K-Ras−GEF interaction and modification of the GTP binding site,[16−18] and (4) targeting potential allosteric regulatory sites.[19,20]

Here, we describe a strategy for targeting oncogenic K-Ras by combining computational methods and biochemical assays. We discovered a potential allosteric binding site, the P110 site, near the C-terminus of K-Ras^{G12D}. The P110 site involves residues Arg97, Asp105, Ser106, Glu107, Asp108, Val109, Pro110, Met111, Tyr137, Gly138, Ile139, Glu162, Lys165, and His166. Using virtual screening, we discovered a candidate P110 site binding compound, termed KAL-21404358. We used biochemical assays to validate the binding of KAL-21404358. A combination of microscale thermophoresis (MST), a thermal shift assay (TSA), line broadening nuclear magnetic resonance (NMR), and heteronuclear single-quantum coherence (HSQC) NMR demonstrated binding of KAL-21404358 to K-Ras^{G12D} with a K_D of 100 μM and allosteric effects on switch I and switch II. KAL-21404358 was further found to disrupt the K-Ras^{G12D}−B-Raf interaction using a NanoBiT split luciferase assay and to impair the Raf-MEK-ERK and PI3K-AKT signaling pathways. We designed analogues to define the structure−activity relationship around the KAL scaffold. These findings suggest that the P110 site may an allosteric regulatory site for targeting oncogenic K-Ras^{G12D}. Moreover, this structure-based approach provides a strategy for discovering small molecule inhibitors for otherwise challenging drug targets.

MATERIALS AND EXPERIMENTAL DETAILS

Software and Computational Methods. Molecular dynamics (MD) simulations, mixed solvent molecular dynamics (MxMD) simulations, molecular docking, and modeling were performed using Maestro (Schrödinger Suite), Molecular Operating Environment (MOE), and PyMOL. Chemical structures were drawn using ChemDraw Professional 16.0. Statistical analyses were performed using Prism 7.0 (GraphPad Software). Libraries of commercially available compounds were compiled from the inventories of Asinex, Enamine, Chembridge, ChemDiv, IBS, Life, Maybridge, and TimTec. A fragment subset of ∼3.5 million compounds was selected and screened.

Protein Data Bank (PDB) structures were imported in Maestro (Schrödinger Suite). Structures were preprocessed, optimized, and minimized using default settings by Protein Preparation Wizard (Schrödinger Suite). SiteMap (Schrödinger Suite) was run using the default setting. MD simulations were performed with Desmond Molecular Dynamics (Schrödinger Suite). The total simulation time was 200 ns. Twenty representative clusters were then generated using the default setting of RMSD Based Clustering Of Frames From Desmond Trajectory (Schrödinger Suite). MxMD simulations were run by scripts. Ten protein cosolvent boxes for each of six probes (acetonitrile, isopropanol, pyrimidine, acetone, imidazole, and *N*-methylacetimide) were first generated by a shell script (see the Supporting Information). MxMD simulations were then performed by a "run_cosolvent_simulations.sh" script (see the Supporting Information). The map was finally generated by "01_generate_occupancy.sh" and "02_generate_maps.sh" scripts (see the Supporting Information).

The P110 site was selected using Receptor Grid Generation (Schrödinger Suite) by specifying residue Pro110 as the center of the enclosing box. No constraints were defined. Different poses of compounds were generated by defining ionization states from pH 4.0 to 7.0 and stereoisomers using LigPrep (Schrödinger Suite). Ligand Docking (Schrödinger Suite) was then used to calculate the Glide Docking Scores. A lower score meant a higher binding affinity. WaterMap (Schrödinger Suite) was run by defining KAL-21404358 ligand docking in the P110 site. The simulation time was 2.0 ns.

Molecular Cloning. The *KRAS*^{G12D} plasmid was previously described.[14] Binding-deficient mutants of the *KRAS*^{G12D} plasmid were generated using a QuikChange XL site-directed mutagenesis kit. Primers were designed using the Agilent QuikChange Primer Design application and purchased from Integrated DNA Technologies: *KRAS*^{G12DR97G} forward primer, 5′ GAA GAT ATT CAC CAT TAT GGA GAA CAA ATT AAA AGA GTT AAG G 3′; *KRAS*^{G12DR97G} reverse primer, 5′ CTT AAC TCT TTT AAT TTG TTC TCC ATA ATG GTG AAT ATC TTC 3′; *KRAS*^{G12DE107A} forward primer, 5′ GAG TTA AGG ACT CTG CAG ATG TAC CTA TGG TCC 3′; *KRAS*^{G12DE107A} reverse primer, 5′ GGA CCA TAG GTA CAT CTG CAG AGT CCT TAA CTC 3′; *KRAS*^{G12DD108A} forward primer, 5′ TAA GGA CTC TGA AGCT GT ACC TAT GGT CC 3′; *KRAS*^{G12DD108A} reverse primer, 5′ ACC ATA GGT AC AGC T TCA GAG TCC TTA ACT C 3′; *KRAS*^{G12DP110D} forward primer, 5′ AGA TGT AGA TAT GGT CCT AG 3′; *KRAS*^{G12DP110D} reverse primer, 5′ AGG ACC ATA TCT ACA TCT TC 3′. DNA sequencing was performed to confirm the amino acid sequence of the construct (GeneWiz).

Protein Expression and Purification. The *KRAS*^{G12D} construct was expressed in *Escherichia coli* BL21-Gold (DE3) cells (Stratagene). An isolated colony was transferred to 8 mL of LB medium with 100 μg/mL ampicillin, and the inoculated culture was incubated while being shaken (225 rpm) at 37 °C for 4.5 h. The starter culture was added to 1 L of fresh LB medium with 100 μg/mL ampicillin. The culture was incubated while being shaken at 37 °C and 225 rpm until the OD_{600} reached 0.6. The temperature was then decreased to 15 °C. Cells were incubated with 500 μM isopropyl β-D-1-thiogalactopyranoside (IPTG) while being shaken at 15 °C and 225 rpm overnight. The next day, the bacteria were harvested by centrifugation at 4000*g* for 20 min at 4 °C and the pellet obtained was ready for purification or stored at −20 °C.

The pellet was resuspended in 25 mL of chilled lysis buffer [10 mM Tris (pH 7.5), 500 mM NaCl, 5 mM $MgCl_2$, 5 mM imidazole, 2 mM TCEP, and Roche protease inhibitor cocktail]. The bacteria were lysed by sonication on ice for 6 min, and the lysate was centrifuged at 15000 rpm for 45 min at 4 °C to remove cell debris. The clarified lysate was incubated with Ni Sepharose 6 Fast Flow beads (GE Life Sciences) on a rotator at 4 °C for at least 1 h. The beads were washed with wash buffer [10 mM Tris (pH 7.5), 500 mM NaCl, 20 mM imidazole, 5 mM $MgCl_2$, and 2 mM TCEP] to remove nonspecific binding. The protein was eluted with 10 mM Tris (pH 7.5), 500 mM NaCl, 250 mM imidazole, 5 mM $MgCl_2$, and 2 mM TCEP. The protein was further purified using a gel filtration Superdex 200 column in FPLC buffer containing 25 mM Tris (pH 7.5), 100 mM NaCl, 5 mM $MgCl_2$, and 2 mM TCEP. The fractions containing K-Ras^{G12D} were pooled together and analyzed by sodium dodecyl sulfate−polyacrylamide gel electrophoresis (SDS−PAGE). The protein concentration was determined using absorbance at 280 nm with an extinction coefficient of 11920 M^{-1} cm^{-1}.

Nucleotide Exchange. Nucleotides in endogenous recombinant K-Ras^{G12D} were exchanged with GDP or

DOI: 10.1021/acs.biochem.8b01300
Biochemistry XXXX, XXX, XXX−XXX

GppNHp using an EDTA loading procedure. K-Ras^{G12D} protein (final concentration of 70 μM) was incubated with a 70-fold molar excess of EDTA (final concentration of 5 mM) and a 70-fold molar excess of new nucleotide (final concentration of 5 mM) for 2 h at 30 °C. After incubation, the sample was placed on ice for 2 min and then $MgCl_2$ was added (final concentration of 65 mM) to stop the reaction. To remove excess unbound nucleotide, the sample was added to a NAP-5 column (GE Life Sciences) equilibrated with FPLC buffer and eluted with FPLC buffer at 100 μL per fraction. Eluted fractions were evaluated using the NanoDrop method to determine protein concentration.

Microscale Thermophoresis (MST). One hundred microliters of 200 nM K-Ras^{G12D} was combined with 100 μL of 100 nM RED-tris-NTA dye in PBS buffer with 3 mM DTT and 0.05% Tween 20 (PBSTD buffer). The protein/dye mixture was incubated at room temperature for 30 min, followed by centrifugation for 10 min at 4 °C and 15000*g*. The compounds were arrayed across a 16-point dilution series in PBSTD buffer and mixed in a 1:1 ratio with a labeled protein solution in a 20 μL volume. The reaction mixture were loaded into standard treated capillaries and analyzed with Monolith NT.115 (Nanotemper Technologies) at 60% LED power and 40% MST power with a laser-on time of 5 s. The K_D was calculated by taking the average of triplicate F_{norm} measurements at each concentration and fitting the data to a sigmoidal four-parameter fitting function in Prism (GraphPad Software). R-Ras, R-Ras2, and Rap1A were purchased from ProSpecBio. K-Ras WT was purchased from Cell Biolabs. H-Ras WT was acquired from Enzo Life Sciences.

Thermal Shift Assay (TSA). A fluorescent thermal shift assay was used to validate the binding and confirm the success of the nucleotide exchange procedure of all GTPases used in the study. The assay was carried out in triplicate in Fast 96-well optical plates containing 5 μM protein and 5× SYPRO Orange dye (Invitrogen) in a total volume of 20 μL/well. Samples were heated at a rate of 3 °C/min from 25 to 95 °C, and protein unfolding was observed by monitoring the fluorescence of SYPRO Orange dye at 470 nm excitation and 623 nm emission using a ViiA7 real-time polymerase chain reaction machine (Applied Biosystems). K-Ras^{G12D} with dimethyl sulfoxide (DMSO) was used on the same plate as a reference for the shift in melting temperature (T_m) with compounds. Each GTPase with an endogenous nucleotide was also used on the same plate as a reference for the shift in melting temperature (T_m) with the new nucleotide. All experiments were performed in triplicate. Data were analyzed using Protein Thermal Shift Software (Applied Biosystems) to determine the T_m of each well.

NMR Line Broadening. For NMR line broadening studies, the samples were buffer exchanged into Milli-Q water using a Millipore spin column (13000*g* for 5 min at 4 °C, repeated five times, each time adding fresh Milli-Q water and discarding the flow-through). Then, 10% D_2O was added to the protein/compound mixtures: protein only, 1:1, 1:3, and compound only. NMR line broadening experiments were performed on Bruker Avance III 500 Ascend (500 MHz) spectrometers (Columbia University) at 298 K. Compound peak assignment was completed using MestReNova version 10.0.2.

HSQC NMR. Uniformly ^{15}N-labeled K-Ras^{G12D} protein without an N-terminal His_6 tag was prepared. The *KRAS*^{G12D} construct was expressed in *E. coli* BL21-Gold (DE3) cells (Stratagene) growing at 37 °C in M9 minimal medium supplemented with 100 μg/mL ampicillin, 2 mM $MgSO_4$, 100 mM $CaCl_2$, 1× trace metals, 1× RPMI 1640 vitamin stock (Sigma-Aldrich, catalog no. R7256), 10 μg/mL biotin, 10 μg/mL thiamine hydrochloride, and 3 g/L $^{15}NH_4Cl$ as the sole nitrogen source. The remaining steps were identical to K-Ras^{G12D} expression and purification described above. Thrombin was then added at a level of 5 units/mg of protein to cleave the N-terminal His_6 tag. The reaction was allowed to proceed overnight at 4 °C. The next day, the protein solution was passed over Ni-Sepharose 6 Fast Flow beads (GE Life Sciences) and the flow-through containing the ^{15}N-labeled K-Ras^{G12D} protein without a histidine tag was concentrated and flash-frozen. The purity was checked by SDS−PAGE.

^{1}H−^{15}N HSQC experiments were performed on Bruker Avance III 500 Ascend (500 MHz) spectrometers (Columbia University) at 298 K. Uniformly ^{15}N-labeled K-Ras^{G12D} was dissolved at concentrations of 100−150 μM in NMR buffer [50 mM HEPES (pH 7.4), 50 mM NaCl, 2 mM $MgCl_2$, 2 mM TCEP, and 10% D_2O]. The ^{1}H carrier frequency was positioned at the water resonance. The ^{15}N carrier frequency was positioned at 115 ppm. Suppression of the water signal was accomplished using the WATERGATE sequence. Heteronuclear decoupling was accomplished using the GARP decoupling scheme. Assignments of K-Ras^{G12D} were previously published.[14] All data were processed and analyzed using TopSpin 3.1 (Bruker) and Sparky (developed by T. D. Goddard and D. G. Kneller, University of California, San Francisco, CA).

NanoBiT Split Luciferase Assay. HEK293T cells from ATCC (catalog no. CRL-1573) were seeded 16 h prior to use in 10% fetal bovine serum (FBS) in Dulbecco's modified Eagle's medium. Plasmids (*KRAS*-SmBiT/*BRAF*-LgBiT or SmBiT/LgBiT positive controls) were transfected into HEK293T cells and incubated for 48−72 h. After transfection was complete, compounds with the indicated concentration were added and treated for 1 h at 37 °C and 5% CO_2. Plates were then read with a Tecan Infinite M200 plate reader for luminescence every 6 min for 3 h at 37 °C. Data were analyzed using Prism 7.0 (GraphPad Software).

Cell-Based K-Ras^{G12D}−Raf RBD Pull Down. LS513 cells from ATCC (catalog no. CRL-2134) were seeded 16 h prior to use in 10% FBS in RPMI-1640. The medium was then aspirated and replaced with serum-free medium containing KAL-21404358, and cells were incubated for 24 h. The medium was removed, washed with cold PBS, lysed, and spun down at 13000 rpm at 4 °C to remove unlysed cells and debris. The lysate was incubated with Raf-1 RBD agarose beads (EMD Millipore) for 2 h with rotation at 4 °C. The solution was then spun down at 1500*g*, and the supernatant removed. The beads were washed twice with PBS, resuspended in 4× SDS, and then analyzed by the Western blotting procedure detailed below.

Western Blots. LS513 cells were seeded in RPMI-1640 and 10% FBS with 1% penicillin and streptomycin (PS) 16 h prior to use. The medium was then aspirated, and compounds were added as solutions in serum-free medium (RPMI-1640 with 1% PS) at the indicated concentration. Following treatment, the medium was aspirated from each dish and cells were washed twice with PBS. Cells were lysed with 70 μL of lysis buffer (RIPA buffer from ThermoFisher, catalog no. 89900, 1 mM EDTA, 1 mM phenylmethanesulfonyl fluoride, 1× Halt protease inhibitor cocktail from ThermoFisher, catalog no. 78430, and 1× Halt phosphatase inhibitor cocktail

DOI: 10.1021/acs.biochem.8b01300
Biochemistry XXXX, XXX, XXX−XXX

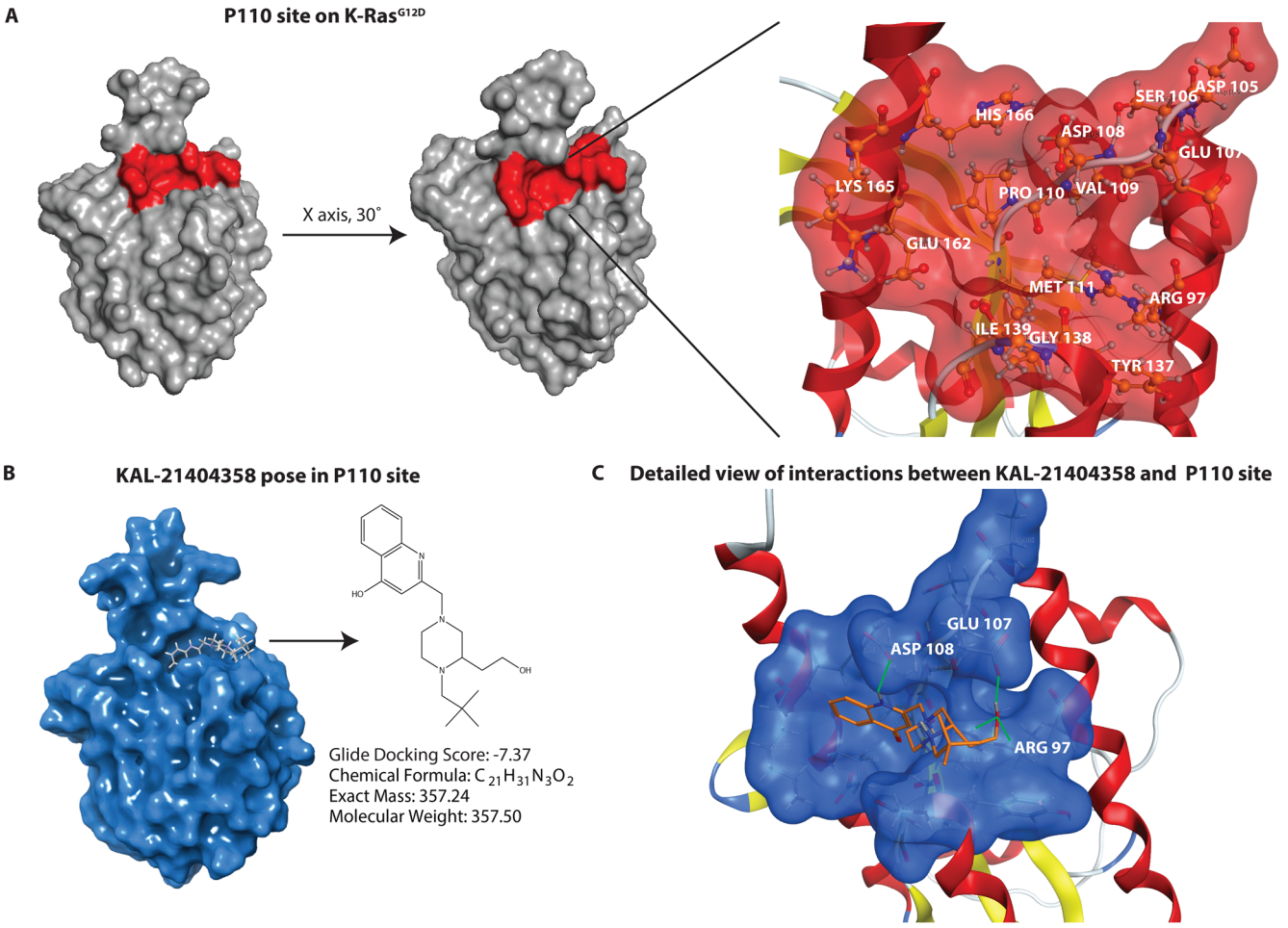

Water ID	ΔG
1	3.84
59	2.73
7	1.45
174	1.19

Figure 1. P110 site and KAL-21404358 binding pose. (A) Model of K-Ras^{G12D} (PDB entry 4DSN) with the P110 site colored red. The P110 site residues are Arg97, Asp105, Ser106, Glu107, Asp108, Val109, Pro110, Met111, Tyr137, Gly138, Ile139, Glu162, Lys165, and His166. (B) KAL-21404358 docking pose in the P110 site and its structure, docking score, chemical formula, mass, and molecular weight. (C) Detailed view of KAL-21404358 binding in the P110 site. Four potential hydrogen bonds are labeled with green lines. (D) KAL-21404358 superimposed with four high-energy water molecules colored red with $\Delta G > 2$ and purple with $\Delta G > 1$.

from ThermoFisher, catalog no. 78426). Unlysed cells and debris were pelleted for 15 min at 16000*g* and 4 °C. Samples were separated using SDS−PAGE and transferred to a polyvinylidene difluoride membrane. The transfer was performed using the iBlot2 system (Invitrogen). Membranes were treated with Li-COR Odyssey blocking buffer for at least 1 h at room temperature and then incubated with a primary antibody (1:1000) in a 1:1 solution of PBS-T (PBS with 0.1% Tween 20) and Li-COR odyssey blocking buffer overnight at 4 °C. Following three 5 min washes in PBS-T, the membrane was incubated with secondary antibodies (1:3000) in a 1:1 solution of PBS-T and Li-COR Odyssey blocking buffer for 1 h at room temperature. Following three 5 min washes in PBS-T, the membrane was scanned using the Li-COR Odyssey Imaging System. Antibodies for pErk1/2, Erk1/2, pAkt Ser473, Akt, pan-Ras (Cell Signaling), and Raf-1 (Santa

DOI: 10.1021/acs.biochem.8b01300
Biochemistry XXXX, XXX, XXX−XXX

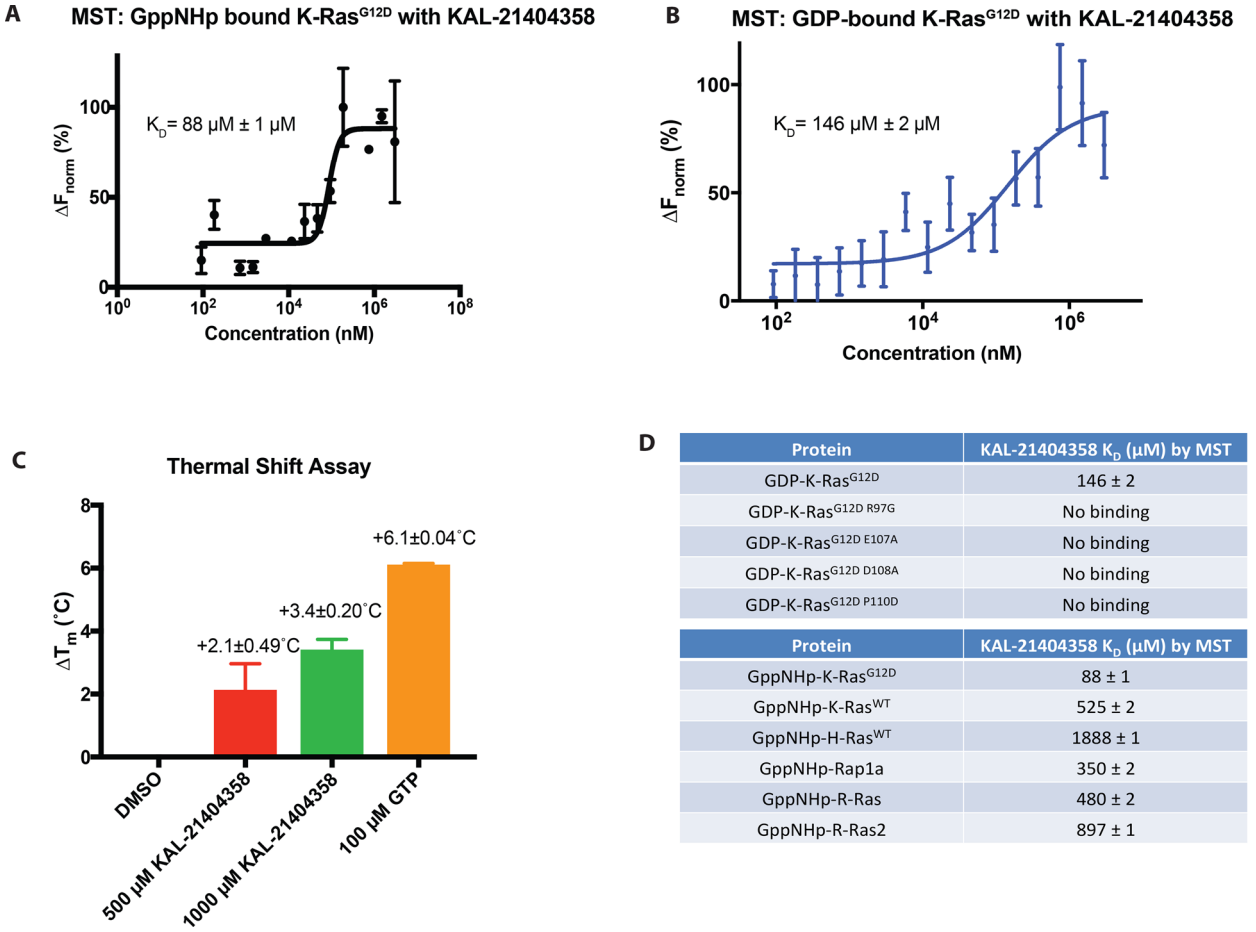

D

Protein	KAL-21404358 K_D (μM) by MST
GDP-K-Ras^{G12D}	146 ± 2
GDP-K-Ras$^{G12D\ R97G}$	No binding
GDP-K-Ras$^{G12D\ E107A}$	No binding
GDP-K-Ras$^{G12D\ D108A}$	No binding
GDP-K-Ras$^{G12D\ P110D}$	No binding

Protein	KAL-21404358 K_D (μM) by MST
GppNHp-K-Ras^{G12D}	88 ± 1
GppNHp-K-Ras^{WT}	525 ± 2
GppNHp-H-Ras^{WT}	1888 ± 1
GppNHp-Rap1a	350 ± 2
GppNHp-R-Ras	480 ± 2
GppNHp-R-Ras2	897 ± 1

Figure 2. Validation of binding of KAL-21404358 to K-Ras^{G12D}. (A) MST assay of KAL-21404358 with GppNHp-bound K-Ras^{G12D} (K_D = 88 ± 1 μM). Data are means ± the standard deviation (SD) of triplicate measurements and are representative of five independent experiments. (B) MST assay of KAL-21404358 with GDP-bound K-Ras^{G12D} (K_D = 146 ± 2 μM) indicating selectivity toward GppNHp-bound vs GDP-bound K-Ras^{G12D}. Data are means ± SD of triplicate measurements and are representative of five independent experiments. (C) KAL-21404358 increases the melting temperature of K-Ras^{G12D} in a thermal shift assay. Data are means ± SD of triplicate measurements and are representative of two independent experiments. (D) KAL-21404358 lacks binding to P110 site mutants and has differential selectivity for K-Ras^{G12D} compared to other RAS family member proteins. Data are means ± SD of triplicate measurements and are representative of one independent experiment.

Cruz) were detected using a goat anti-rabbit or goat anti-mouse IgG antibody conjugated to an IRdye at 800CW and 680CW, respectively (Li-COR Biosciences).

RESULTS

Discovery of the P110 Site and KAL-21404358. Given the challenges of directly targeting the nucleotide binding site and effector interaction surface, we hypothesized there might be allosteric pockets regulating the on and off cycle of K-Ras. To identify such sites, we first performed computational analysis of the K-Ras^{G12D} crystal structure (PDB entry 4DSN) using the SiteMap (Schrödinger Suites) prediction tool.[21,22] The P110 site had the highest score for a potential small molecule binding site (r_sitemap_SiteScore = 0.92) and identified a binding site including residues Arg97, Asp105, Ser106, Glu107, Asp108, Val109, Pro110, Met111, Tyr137, Gly138, Ile139, Glu162, Lys165, and His166 (Figure 1A, colored red).

To explore the potential robustness of the P110 site across different protein conformations, we conducted similar analyses of other crystal structures of K-Ras (PDB entries 4EPR and 4OBE) and other Ras isoforms H-Ras (PDB entry 4L9W) and N-Ras (PDB entry 3CON). We found that the P110 site still appeared across these structures, but the SiteMap scores were not as high as in structure 4DSN (Figure S1A). This indicates that the P110 site is more apparent in GTP-bound K-Ras^{G12D} than in GDP-bound K-Ras^{G12D}. Computational analysis of the P110 site on 4DSN (orange) and 4EPR (blue) showed different poses of residues Arg97, Asp105, Ser106, Glu107, Asp108, and Lys165 (Figure S1B). These conformational changes make the P110 site on GTP-bound K-Ras^{G12D} open and larger than those on GDP-bound K-Ras^{G12D}. Comparison of P110 sites of 4DSN (orange) with those of 4L9W (green) showed different poses of residues Asp105, Ser106, Glu107, Asp108, Pro110, and Met111, making the P110 site open and larger in K-Ras (Figure S1C). These observations suggest that the P110 site is specific to K-Ras and is not as apparent in H-Ras or N-Ras, at least in the X-ray structures currently available.

Next, we performed a molecular dynamics (MD) simulation to mimic different conformations of K-Ras^{G12D} other than the ones found in the crystal structures. Twenty clusters were generated from a 200 ns MD simulation. The P110 site appeared consistently in these simulations, of which one cluster (#6) showed the best SiteMap score of 1.06 (Figure

DOI: 10.1021/acs.biochem.8b01300
Biochemistry XXXX, XXX, XXX−XXX

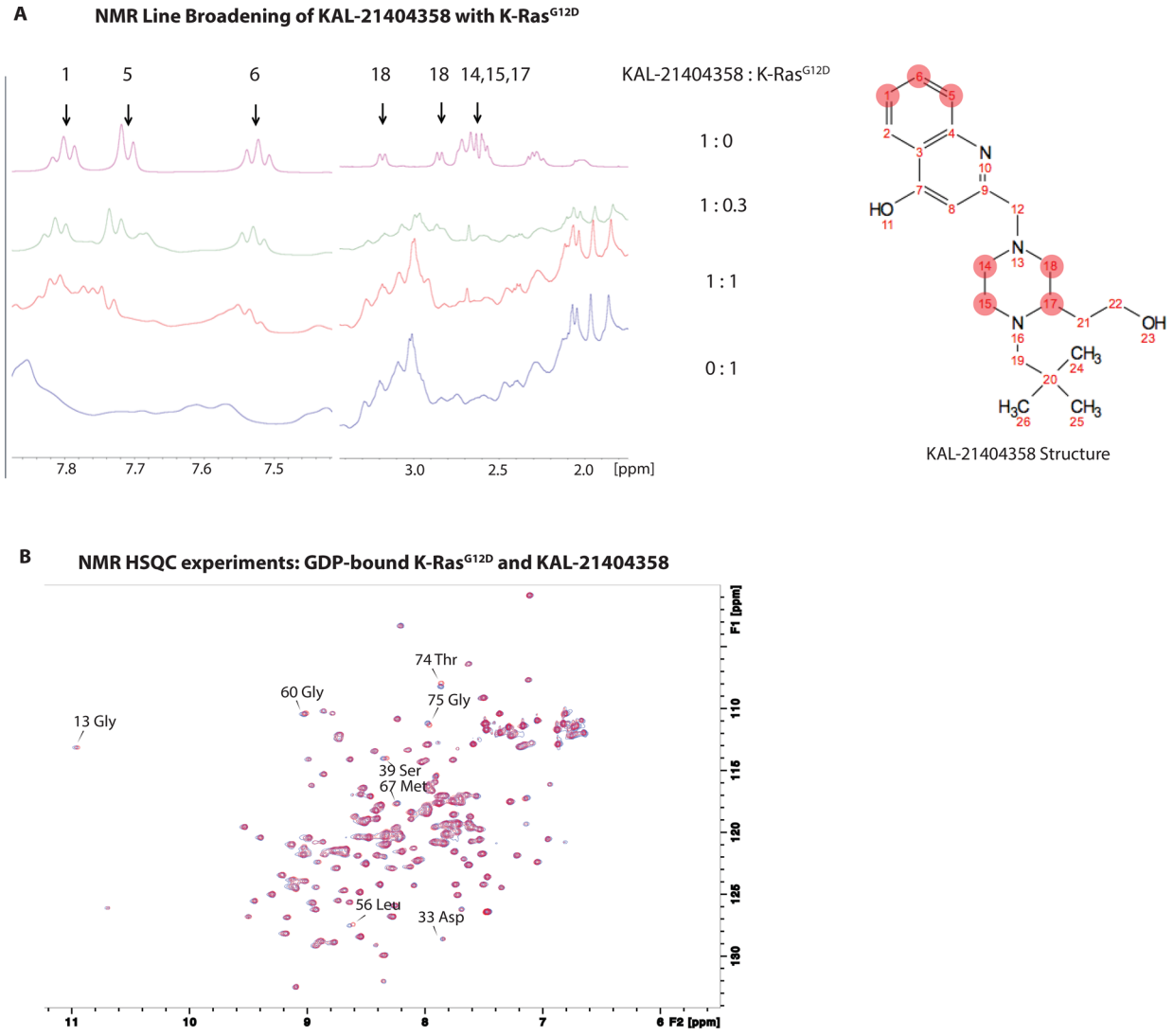

Figure 3. NMR validation of binding of KAL-21404358 to K-Ras^{G12D}. (A) NMR line broadening experiment of KAL-21404358 with an increased concentration of K-Ras^{G12D} (1:0, 1:0.3, 1:1, and 0:1 ratios). Peaks of hydrogens of quinolinol and the piperazinyl group (colored red) were broadened, indicating KAL-21404358's binding to K-Ras^{G12D}. (B) HSQC NMR experiment showing conformational changes in switch I and switch II of K-Ras^{G12D}, which could be explained by P110 site's allosteric effect. Blue represents GDP-bound K-Ras^{G12D} and red represents GDP-bound K-Ras^{G12D} with KAL-21404358 at a 1:7 concentration ratio. Residues changed upon binding with KAL-21404358 are labeled.

S1D). This suggests that this pocket can become even more accessible during the motion of the K-Ras^{G12D} protein.

MxMD simulations were then run with structure 4DSN using acetonitrile, isopropanol, pyrimidine, acetone, imidazole, and *N*-methylacetamide as organic probes. These organic probes can affect the conformation of K-Ras^{G12D} and reveal which sites can be accessible to small molecules of various chemotypes.[23,24] The P110 site was found to contain all of these solvents as a hot spot, indicating its potential as a binding pocket for small organic molecules (Figure S1E).

We evaluated whether we could identify fragments or leadlike compounds predicted to bind with reasonable affinity to the P110 site. We tested 3.5 million compounds using the Glide docking algorithm (Schrödinger Suites), which generates a score in which the more negative the score, the higher the predicted affinity.[25] Seventy-seven fragments with scores of less than −6.5 were obtained for further validation. Four rounds of biochemical screening using MST, a TSA, NMR line broadening, and HSQC NMR spectroscopy were used to select promising compounds from among these 77 candidates. KAL-21404358 was the most favorable compound, as it showed positive binding results in all four tests (Figures 1−3).

KAL-21404358 was predicted to interact well with the P110 site, with a Glide docking score of −7.37 (Figure 1B). A closer view of KAL-21404358 in the P110 site showed four potential hydrogen bonds (between the −NH in the hydroxyquinoline and the carboxyl group of Asp108, between the −OH in the hydroxyethyl group and the carboxyl group of Glu107, and two between the −OH in the hydroxyethyl group and the amine group of Arg97) as well as strong polar interactions (between the bridge of KAL-21404358 and the amide group of Glu107 and between the piperazinyl group and the amide group of Gly138) (Figure 1C).

WaterMap (Schrödinger Suite) was then used to estimate changes in the thermodynamic properties resulting from water molecule displacement by fragments binding in the P110 site.[26,27] Four high-energy water molecules were predicted to be located in the P110 pocket superimposed upon KAL-21404358, which suggested that displacement of these water

DOI: 10.1021/acs.biochem.8b01300
Biochemistry XXXX, XXX, XXX−XXX

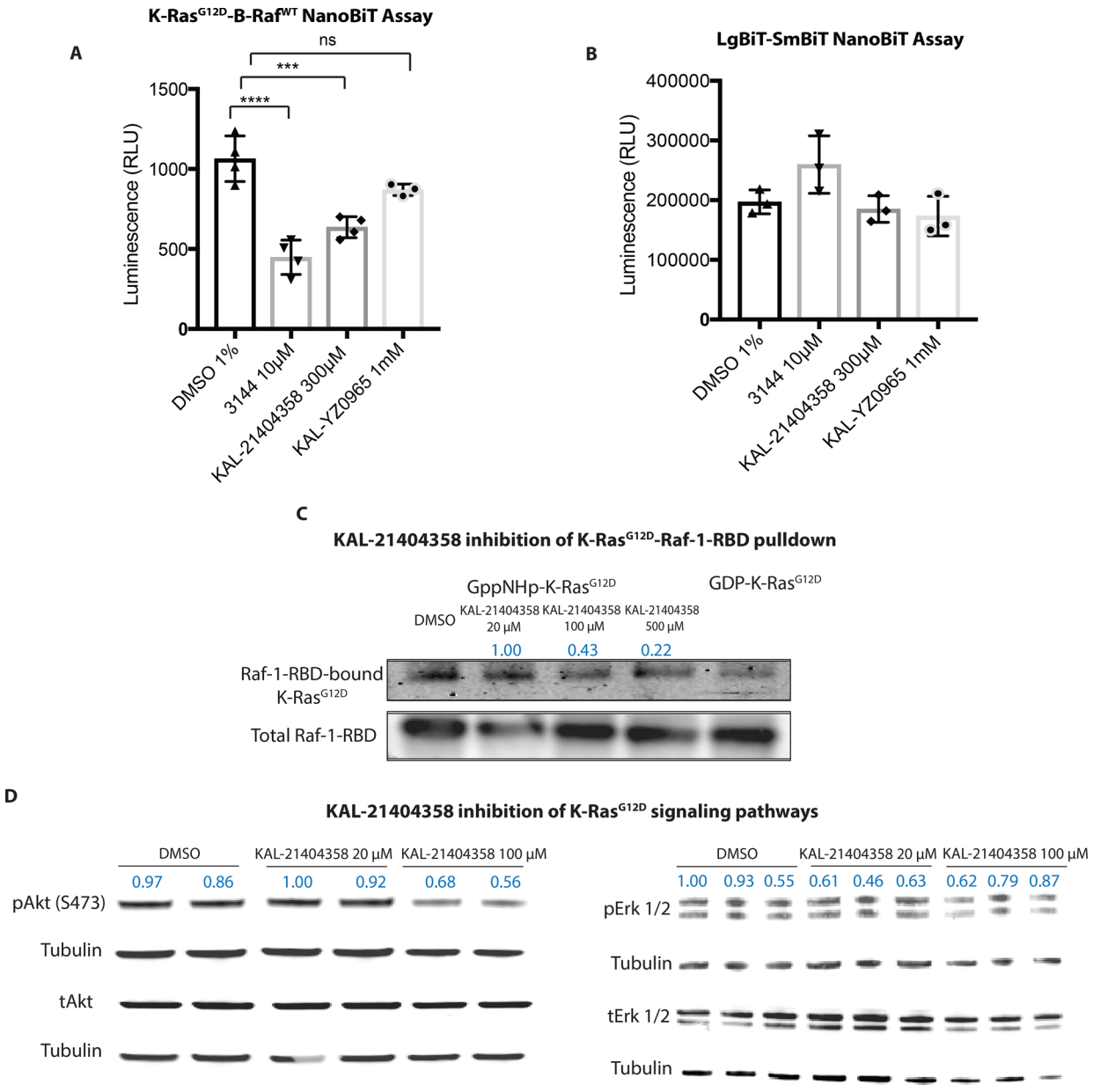

Figure 4. KAL-21404358 inhibits the K-Ras^{G12D}−B-Raf interaction and K-Ras^{G12D}-dependent signaling. (A) A NanoBiT split luciferase assay showed that KAL-21404358 and its analogue KAL-YZ0965 disrupted the K-Ras^{G12D}−B-Raf interaction. 3144 was used as a positive control. K-Ras^{G12D} was fused to SmBiT; B-Raf was fused to LgBiT, and constructs were transfected in HEK293T cells. Luminescent signals were detected when K-Ras^{G12D} bound to B-Raf. Ordinary one-way analyses of variance were conducted in Prism 7. Four asterisks indicate $p < 0.0001$. Three asterisks indicate $p < 0.001$. ns indicates $p > 0.05$. Data are means ± SD of quadruplicate measurements and are representative of three independent experiments. (B) KAL-21404358, KAL-YZ0965, and 3144 were screened against SmBiT-LgBiT to rule out nonspecific inhibition and toxicity. Data are means ± SD of triplicate measurements and are representative of three independent experiments. (C) LS513 cells (with K-Ras^{G12D}) were treated with KAL-21404358 as indicated, and the amounts of Raf-1−RBD-bound K-Ras^{G12D} proteins were determined. Data are representative of two independent experiments. (D) Effects of KAL-21404358 on the abundance of phosphorylated Akt and total Akt (left) and phosphorylated Erk and total Erk (right) were determined at the indicated concentrations in LS513 cells (with K-Ras^{G12D} mutations). LS513 cells from ATCC (catalog no. CRL-2134) were seeded 16 h prior to use in 10% FBS in RPMI-1640. The medium was then aspirated and replaced with serum-free medium containing KAL-21404358, and cells were incubated for 24 h. Relative intensities of phosphorylated forms vs total forms were quantified and are labeled. Data are representative of two independent experiments.

molecules would improve the binding affinity of KAL-21404358 even further (Figure 1D).

Validation of Binding of KAL-21404358 to K-Ras^{G12D}. MST and TSA were used as first-line screening methods. The K_D of KAL-21404358 for GppNHp-bound K-Ras^{G12D} was 88 μM, and the K_D with GDP-bound K-Ras^{G12D} assessed by MST was 146 μM (Figure 2A,B). This suggests that KAL-21404358 has a slightly higher binding affinity for the GppNHp-bound form of K-Ras^{G12D}. TSA experiments confirmed a 2.1 °C melting temperature shift, indicating binding of KAL-21404358 stabilizes GDP-bound K-Ras^{G12D} to thermal denaturation, possibly further inhibiting activation of GDP-K-Ras^{G12D} (Figure 2C). The binding of KAL-21404358 to

DOI: 10.1021/acs.biochem.8b01300
Biochemistry XXXX, XXX, XXX−XXX

Table 1. Analysis and Optimization of the KAL-21404358 Structure–Activity Relationship[a]

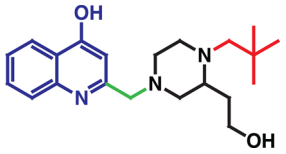

Compound	Structure	MST K_D (μM)
KAL-53051204	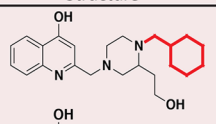	No binding
KAL-74550618	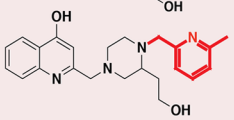	493 *No apparent chemical shifts in HSQC NMR
KAL-10142218	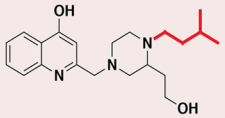	236
KAL-34786714	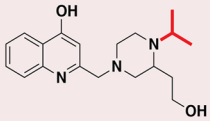	179 *No apparent chemical shifts in HSQC NMR
KAL-27951991	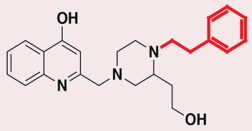	498
KAL-20883404	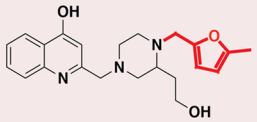	580
KAL-32632258	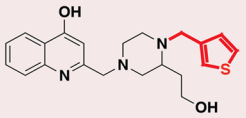	399

Compound	Structure	MST K_D (μM)
KAL-PHB6001	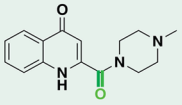	No binding
KAL-PHB6002	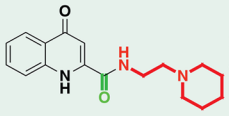	**26 *No apparent chemical shifts in HSQC NMR**
KAL-PHB6003	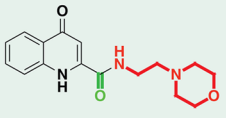	**11 *No apparent chemical shifts in HSQC NMR**
KAL-2241124388	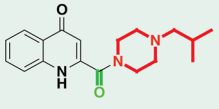	**30 *Chemical shifts in HSQC NMR**

Compound	Structure	MST K_D (μM)
KAL-31672316	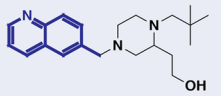	169
KAL-11067146	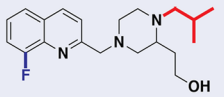	**51 *No apparent chemical shifts in HSQC NMR**
KAL-11096175	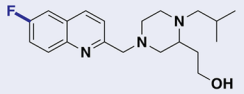	167
KAL-26193929	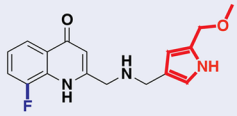	No binding
KAL-84077290	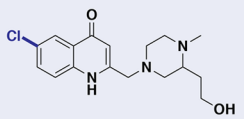	411
KAL-55883121	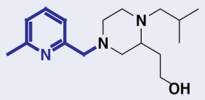	**104**

Compound	Structure	MST K_D (μM)
KAL-YZ0965	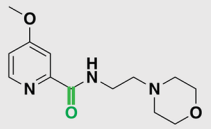	**106 *Chemical shifts in HSQC NMR**
KAL-YZ0968	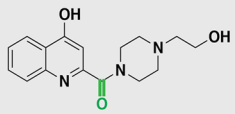	**40 *Chemical shifts in HSQC NMR**
KAL-YZ0970	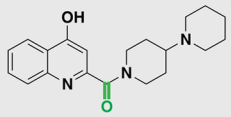	**7 *Chemical shifts in HSQC NMR**

[a]Four functional groups are labeled: hydroxyquinoline in blue, bridge in green, amine group in black, and neopentyl group in red. KAL-21404358 analogue names, structures, and K_D values measured by MST and HSQC NMR are shown. More active compounds are shown in bold.

GppNHp-bound K-Ras^{G12D} did not cause a temperature shift (Figure S2A).

To test whether KAL-21404358 bound specifically to the P110 site, we constructed four mutants predicted to be deficient for binding to KAL-21404358: R97G, E107A,

DOI: 10.1021/acs.biochem.8b01300
Biochemistry XXXX, XXX, XXX–XXX

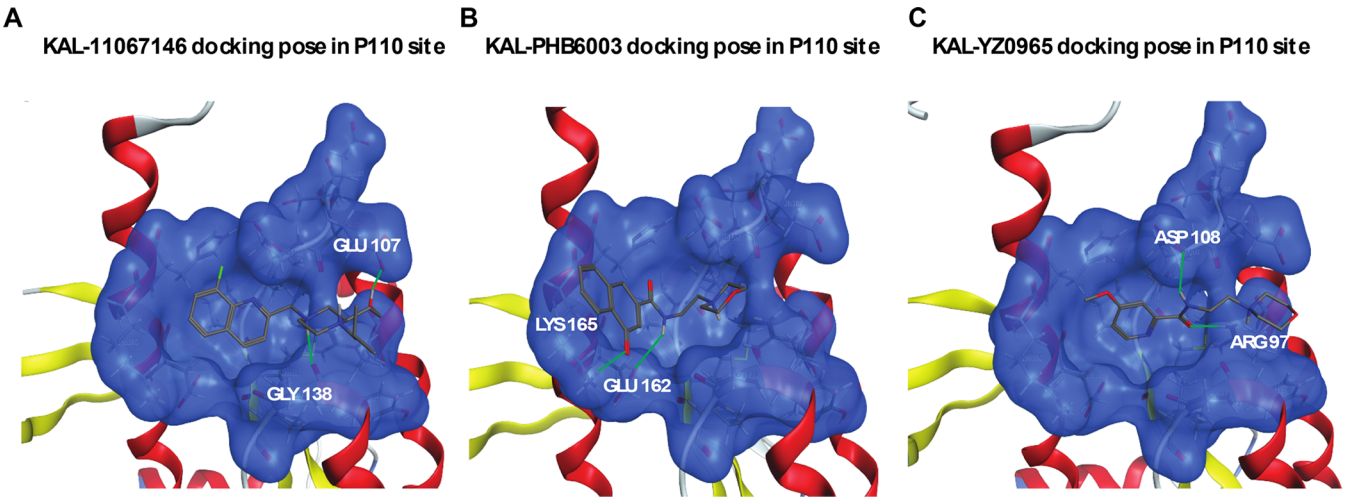

Figure 5. Computational docking poses of three representative analogues of KAL-21404358. (A) KAL-11067146 docking pose in the P110 site. KAL-11067146 has a docking pose similar to that of KAL-21404358. Addition of a fluorine molecule did not improve the binding of KAL-11067146 to the receptor. Potential hydrogen bonds are labeled with green lines. (B) KAL-PHB6003 has a reverse docking pose compared to that of KAL-21404358. Potential hydrogen bonds are labeled with green lines. (C) KAL-YZ0965 has a docking pose similar to that of KAL-21404358. Addition of a carbonyl group to the bridge helps form an additional hydrogen bond to improve KAL-YZ0965 binding. Potential hydrogen bonds are represented with green lines.

D108A, and P110D. No binding between KAL-21404358 and these four mutants was detected using MST, supporting the hypothesis that this compound binds in the P110 site (Figure 2D; the original MST curves are shown in Figure S2B). We also examined the specificity of KAL-21404358 for K-Ras^{G12D} over K-Ras^{WT}, H-Ras^{WT}, Rap1a, R-Ras, and R-Ras2. Each protein was tested for its ability to bind to KAL-21404358 using MST. Much weaker binding of KAL-21404358 was detected toward these other proteins, suggesting that KAL-21404358 has selectivity for K-Ras^{G12D} (Figure 2D; the original MST curves are shown in Figure S2C).

Validation of the KAL-21404358 Binding Site and Binding Mode. To further elucidate how KAL-21404358 binds to K-Ras^{G12D}, we used NMR line broadening. The disappearance of hydrogens 1, 5, 6, 14, 15, 17, and 18 in the ^{1}H NMR spectrum of the compound indicated binding to K-Ras^{G12D}, which is likely due to these being the interacting atoms on KAL-21404358 (Figure 3A). Analysis of the structure of KAL-21404358 suggested that it bound to K-Ras^{G12D} with the quinolinol and piperazinyl group, but not the neopentyl group, which was consistent with the computational prediction.

HSQC NMR was then used to identify the residues on K-Ras^{G12D} that change upon KAL-21404358 binding to test for possible allosteric effects. Conformational changes in the switch I and switch II regions (Asp33, Ser39, Leu56, Gly60, Met 67, Thr74, and Gly75) were observed in GDP-bound K-Ras^{G12D} (Figure 3B) upon KAL-21404358 binding, suggesting an allosteric effect on the K-Ras^{G12D} conformation. However, KAL-21404358 interacted with only side chains of residues, as no backbone shifts near the P110 residues were observed in the HSQC NMR experiments.

Inhibition of the K-Ras^{G12D}−B-Raf Interaction. On the basis of KAL-21404358's binding mode, we tested whether this compound could disrupt the interaction between K-Ras^{G12D} and B-Raf using a NanoBiT split luciferase assay.[28] K-Ras^{G12D} was fused to SmBiT, and B-Raf was fused to LgBiT. The Ras−Raf interaction inhibitor 3144 was used as a positive control for disruption of the interaction.[14] KAL-21404358 and its analogue, KAL-YZ0965, exhibited a luminescence lower than that of DMSO-treated control samples, suggesting that these compounds disrupted the K-Ras^{G12D}−B-Raf interaction (Figure 4A). KAL-21404358 is more effective at lower concentrations, whereas KAL-YZ0965's effectiveness was low. The compounds were simultaneously tested in cells with SmBiT/LgBiT to rule out nonspecific inhibition (Figure 4B). A K-Ras^{G12D}−Raf-1−RBD pull-down assay was also conducted to validate disruption of this interaction. Less K-Ras^{G12D} was bound to Raf-1−RBD beads in the presence of KAL-21404358, which supported the hypothesis that this compound disrupts this interaction in cells (Figure 4C).

Next, the effect of KAL-21404358 on downstream Raf-Mek-Erk and PI3K-Akt-mTor pathways was investigated. Less cellular phosphorylated Akt and phosphorylated Erk were detected after treatment of cells with KAL-21404358 (Figure 4D). However, the inhibitory effect of KAL-21404358 in the pull-down and Western assays was not strong, consistent with a low binding affinity. Further optimization of this compound or other compounds that bind in this site is needed to enable efficient allosteric inhibition of K-Ras^{G12D} in cells.

Modification of the KAL-21404358 Scaffold. To optimize the properties of KAL-21404358, we designed and synthesized a series of close structural analogues. We divided KAL-21404358 into four functional groups: the hydroxyquinoline (blue), the bridge (green), the amine group (black), and the neopentyl group (red) (Table 1). First, we hypothesized that the neopentyl group might be replaced to improve properties of the compounds, because (1) it did not interact with the P110 pocket in the computational models and (2) this group is hydrophobic, decreasing the aqueous solubility of the compound. We thus identified and tested seven KAL-21404358 analogues (red background) that had replacements of the neopentyl group only. The binding affinities of these compounds, as assessed by MST, were not improved, consistent with a lack of interaction at this site. These replacements did not generate new interactions between compounds and the receptor, likely because this group is facing the solvent. We next focused our attention on the

DOI: 10.1021/acs.biochem.8b01300
Biochemistry XXXX, XXX, XXX−XXX

A

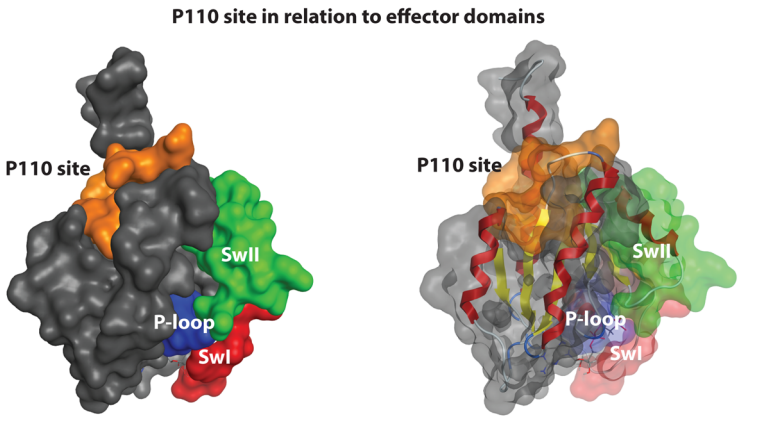

B

Functional sites	Residues
P110 site	Arg97, Asp105, Ser106, Glu107, Asp108, Val109, Pro110, Met111, Tyr 137, Gly138, ILE139, Glu162, Lys165, and His166.
P-loop	Gly10, Ala11, Asp12, Gly13, Val14, Gly15, Lys16, Ser17
Switch I	Asp30, Glu31, Tyr32, **Asp33**, Pro34, Thr35, Ile36, Glu37, Asp38, **Ser39**, Tyr40
Switch II	**Gly60**, Gln61, Glu62, Glu63, Tyr64, Ser65, Ala66, **Met67**, Arg68, Asp69, Gln70, Tyr71, Met72, Arg73, **Thr74**, **Gly75**, Glu76
Allosterically affected with binding of KAL-21404358	**Asp33, Ser39, Leu56, Gly60, Met67, Thr74 and Gly75**

Figure 6. Location of the P110 site in relation to effector domains. (A) The P110 site (orange) is in the allosteric lobe, opposite the functional P loop (blue), switch I (red), and switch II (green) domains that constitute the active site for GTP hydrolysis and effector protein binding. The left one shows the surface, whereas the right one shows the structure. (B) Residues in the P110 site, P loop, switch I, and switch II and those allosterically affected with binding of KAL-21404358 are listed and compared. Key residues that undergo conformational changes upon binding are shown in bold.

hydroxyquinoline moiety, which fits well into the P110 pocket. Our hypothesis was that adding functional groups or changing the hydroxyquinoline moiety might form new hydrogen bonds between KAL-21404358 analogues and K-Ras^{G12D}, thereby improving binding. Six KAL-21404358 analogues (blue background) were identified and tested, among which analogue KAL-11067146 (bold) showed more potent binding in the MST assay (Table 1). However, this analogue did not affect the K-Ras^{G12D} conformation in an HSQC NMR experiment, suggesting a loss of allosteric inhibitory activity. Computational docking did not show the presence of a hydrogen bond formed by the addition of the fluorine (Figure 5A), consistent with the NMR result.

Next, we added a carbonyl group to the bridge region to increase the number of hydrogen bond interactions with K-Ras^{G12D} and also to increase the hydrophilicity of KAL-21404358. Considering the difficulty of synthesizing the hydroxyethyl piperazinyl moiety, we decided to replace it with other cyclic amines. Three analogues were synthesized, and one was commercially available, among which KAL-PHB6002, KAL-PHB6003, and KAL-2241124388 exhibited more potent binding in the MST assay. Computational docking showed a reverse pose for KAL-PHB6003 in the P110 site as an example of this series of analogues (Figure 5B). Two potential hydrogen bonds are likely to be formed between the oxygen molecule of the hydroxyquinoline and the amine group of Lys165 as well as between the amine group of the bridge and the carboxyl group of Glu162. However, HSQC NMR experiments again showed the lack of an allosteric inhibitory effect of KAL-PHB6002 and KAL-PHB6003. The chemical shifts (Asp33, Ser39, Leu56, and Gly75) of binding of KAL-2241124388 to K-Ras^{G12D} were the same with KAL-21404358 (Figure S3A). No backbone chemical shifts of the P110 site were observed. The NanoBiT split luciferase assay showed a trend toward a weaker luminescence signal in the presence of KAL-2241124388 (Figure S3B).

We further synthesized 15 analogues with carbonyl bridges and cyclic amines (see the supplementary methods in the Supporting Information). Three of these compounds (KAL-YZ0965, KAL-YZ0968, and KAL-YZ0970, gray background and bold) exhibited higher binding affinity as determined by MST and chemical shifts in HSQC NMR experiments (Table 1). The chemical shifts of these compounds in HSQC NMR experiments were similar to those of KAL-21404358 but not as apparent (Figure S3A). No backbone chemical shifts of the P110 site were observed. Computational docking showed that KAL-YZ0965 fit well into the P110 site, as an example of this series of analogues. The addition of an amide group as the bridge could form two potential hydrogen bonds with K-Ras^{G12D}, stabilizing the binding of KAL-YZ0965 (Figure 5C). KAL-YZ0965, KAL-YZ0968, and KAL-YZ0970 together with KAL-55883121 (similar and better binding affinity with KAL-21404358 in the MST assay) were thus selected for testing in the NanoBiT K-Ras^{G12D}–B-Raf interaction assay. We detected

DOI: 10.1021/acs.biochem.8b01300
Biochemistry XXXX, XXX, XXX−XXX

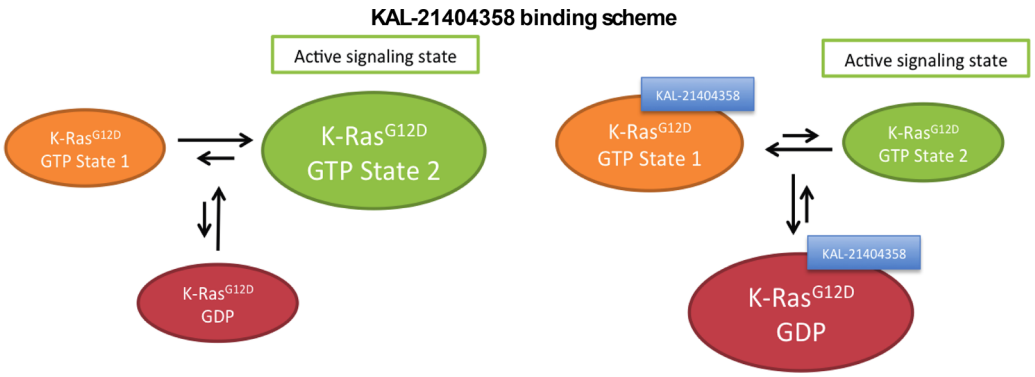

Figure 7. KAL-21404358 binding scheme. The orange ellipse represents inactive GTP-bound K-Ras^{G12D} (state 1). The green circle represents active GTP-bound K-Ras^{G12D} (state 2). The red ellipse represents inactive GDP-bound K-Ras^{G12D}. The size of the circles represents the relative amounts of different K-Ras^{G12D} states. In the absence of KAL-21404358, K-Ras^{G12D} favors the active state 2 conformation. When KAL-21404358 binds to GTP-bound K-Ras^{G12D}, it stabilizes state 1, disrupting the binding of effectors. When KAL-21404358 binds to GDP-bound K-Ras^{G12D}, it traps the protein in this inactive state, thereby reducing the amount of active-state protein.

trends toward weaker luminescence signals in the presence of KAL-YZ0965, KAL-YZ0968, and KAL-55883121 (Figure 4 and Figure S3B). Moreover, KAL-YZ0965, KAL-YZ0968, and KAL-YZ0970 have improved aqueous solubility, which provides opportunities for future studies with these compounds (Figure 4 and Figure S3B).

DISCUSSION

K-Ras^{G12D} has been considered a challenging target over the past 30 years. Here, we explore a strategy for discovering small molecule inhibitors that directly bind to this oncogenic K-Ras mutant. This strategy started with computational design, leading to discovery of a potential binding pocket. The P110 site is in the allosteric lobe, which is opposite of the functional P loop (phosphate binding loop, residues 10−17), switch I (effector binding region, residues 30−40), and switch II (effector binding region and GEF and GAP binding region, residues 60−75) regions, which constitute the active site for GTP hydrolysis and interaction sites for effector proteins, including Raf, PI3K, RalGDS, and GAP (Figure 6A).[29,30] Despite the distance from the P110 site to effector domains, residues in switch I and switch II undergo conformational changes upon binding of KAL-21404358, causing disruption of K-Ras^{G12D} signaling activity (Figure 6B).

We used a tiered set of computational and biochemical assays to evaluate whether compounds can bind to this site and, if so, what effect they have on the K-Ras^{G12D} protein. The first-line screening consisted of computational ligand docking to select compounds predicted to bind in this site. The second screening filter involved the use of MST and TSA to validate binding to K-Ras^{G12D} experimentally. The third tier was NMR line broadening and a HSQC NMR binding assay to further discover the binding mode and location and to assess allosteric effects of binding. The fourth tier was a Ras functional assay involving direct interactions with Raf and two well-established cellular signaling pathways.

KAL-21404358 was found to be the best candidate from this set of assays. KAL-21404358 was further validated to specifically bind to K-Ras^{G12D} in the P110 site. Although the binding affinity was moderate, KAL-21404358 was able to disrupt the K-Ras−B-Raf interaction and Akt and Erk signaling pathways at high concentrations. GTP-bound K-Ras^{G12D} exists in two distinct conformations, state 1 and state 2, where state 1 has a lower binding affinity for effectors.[31−33] On the basis of our experimental results, we hypothesize that KAL-21404358 binds to GTP-bound K-Ras^{G12D} state 1 and thus shifts the protein equilibrium from state 2 toward state 1 (Figure 7). KAL-21404358 can also bind to the GDP-bound (inactive) conformation with a 2-fold lower affinity. We hypothesize that KAL-21404358 stabilizes and traps K-Ras^{G12D} in this inactive GDP-bound state by reducing its probability to nucleotide exchange, thus decreasing the amount of GTP-bound K-Ras^{G12D} (Figure 7). Thus, the P110 pocket, according to this model, is slightly more pronounced in state 1 of the GTP-bound protein but is also present in the GDP-bound protein.

To optimize this scaffold, a high-resolution structure is likely needed. We attempted to obtain such a co-crystal structure without success, likely due to the low binding affinity and low solubility of KAL-21404358. Nonetheless, we did synthesize a series of analogues to define the structure−activity relationship and found that addition of a carbonyl group to the bridge enhances the binding affinity because of the formation of new hydrogen bonds and increases the hydrophilicity of KAL-21404358. The binding affinities of those analogues were improved as shown by the MST assay, but their ability to disrupt K-Ras−B-Raf interaction was not enhanced. This remains to be studied further, especially by using structural biology approaches.

In summary, these findings suggest that the P110 site is a potential allosteric regulatory site for targeting oncogenic K-Ras proteins. KAL-21404358 is the first small molecule candidate for this site. This provides a new strategy for discovering small molecule allosteric inhibitors of KRAS^{G12D}.

ASSOCIATED CONTENT

Supporting Information

The Supporting Information is available free of charge on the ACS Publications website at DOI: 10.1021/acs.biochem.8b01300.

MxMD simulation script, shell script, synthesis of KAL-21404358 analogues, and Figures S1−S3 (PDF)

AUTHOR INFORMATION

Corresponding Author

*E-mail: bstockwell@columbia.edu.

ORCID

Brent R. Stockwell: 0000-0002-3532-3868

DOI: 10.1021/acs.biochem.8b01300
Biochemistry XXXX, XXX, XXX−XXX

Author Contributions

H.F., J.M.C., and B.R.S. designed, performed, and analyzed the results of computational analyses. H.F. and B.R.S. designed, performed, and analyzed the results of molecular cloning, protein expression, purification, MST, TSA, NMR, and cell culture studies. B.R.S., P.H.B., and Y.Z. designed, performed, and analyzed the results of synthetic chemistry. B.R.S. and M.M.D. designed, performed, and analyzed the results of the NanoBiT split luciferase assay. B.R.S. supervised the project. H.F. and B.R.S. wrote the manuscript, with input from other authors.

Funding

This research was supported by grants to B.R.S. from the National Cancer Institute (R35CA209896 and P01CA087497). M.M.D. was supported by the Arnold and Mabel Beckman Foundation.

Notes

The authors declare the following competing financial interest(s): Y.Z., P.H.B., and J.M.C. are now employees of Schrodinger, LLC. B.R.S. holds equity in and consults with Inzen Therapeutics.

■ ACKNOWLEDGMENTS

The authors thank John Decatur and the Columbia Chemistry NMR core facility (National Science Foundation Grant CHE 0840451 and National Institutes of Health Grant 1S10RR025431-01A1) for assistance with compound characterization, Anna Kaplan for assistance with MST and NMR experiments, and Neel Shah for helpful discussions.

■ REFERENCES

(1) Ostrem, J. M., and Shokat, K. M. (2016) Direct small-molecule inhibitors of KRAS: from structural insights to mechanism-based design. *Nat. Rev. Drug Discovery 15*, 771−785.

(2) Boguski, M. S., and McCormick, F. (1993) Proteins regulating Ras and its relatives. *Nature 366*, 643−654.

(3) Hall, B. E., Bar-Sagi, D., and Nassar, N. (2002) The structural basis for the transition from Ras-GTP to Ras-GDP. *Proc. Natl. Acad. Sci. U. S. A. 99*, 12138−12142.

(4) Rajalingam, K., Schreck, R., Rapp, U. R., and Albert, Š. (2007) Ras oncogenes and their downstream targets. *Biochim. Biophys. Acta, Mol. Cell Res. 1773*, 1177−1195.

(5) Pylayeva-Gupta, Y., Grabocka, E., and Bar-Sagi, D. (2011) RAS oncogenes: weaving a tumorigenic web. *Nat. Rev. Cancer 11*, 761−774.

(6) Cox, A. D., and Der, C. J. (2010) Ras history: The saga continues. *Small GTPases. 1*, 2−27.

(7) Cox, A. D., Fesik, S. W., Kimmelman, A. C., Luo, J., and Der, C. J. (2014) Drugging the undruggable RAS: Mission possible? *Nat. Rev. Drug Discovery 13*, 828−851.

(8) Fort, J. G., and Cowchock, S. (1990) Comment on the letter by Hughes et al. *Arthritis Rheum. 33*, 607.

(9) Hopkins, A. L., and Groom, C. R. (2002) The druggable genome. *Nat. Rev. Drug Discovery 1*, 727−730.

(10) Janes, M. R., Zhang, J., Li, L. S., Hansen, R., Peters, U., Guo, X., Chen, Y., Babbar, A., Firdaus, S. J., Darjania, L., Feng, J., Chen, J. H., Li, S., Li, S., Long, Y. O., Thach, C., Liu, Y., Zarieh, A., Ely, T., Kucharski, J. M., Kessler, L. V., Wu, T., Yu, K., Wang, Y., Yao, Y., Deng, X., Zarrinkar, P. P., Brehmer, D., Dhanak, D., Lorenzi, M. V., Hu-Lowe, D., Patricelli, M. P., Ren, P., and Liu, Y. (2018) Targeting KRAS Mutant Cancers with a Covalent G12C-Specific Inhibitor. *Cell 172*, 578−589.e17.

(11) Zeng, M., Lu, J., Li, L., Feru, F., Quan, C., Gero, T. W., Ficarro, S. B., Xiong, Y., Ambrogio, C., Paranal, R. M., Catalano, M., Shao, J., Wong, K. K., Marto, J. A., Fischer, E. S., Janne, P. A., Scott, D. A., Westover, K. D., and Gray, N. S. (2017) Potent and Selective Covalent Quinazoline Inhibitors of KRAS G12C. *Cell Chem. Biol. 24*, 1005−1016.e3.

(12) Lito, P., Solomon, M., Li, L. S., Hansen, R., and Rosen, N. (2016) Allele-specific inhibitors inactivate mutant KRAS G12C by a trapping mechanism. *Science 351*, 604−608.

(13) Trinh, T. B., Upadhyaya, P., Qian, Z., and Pei, D. (2016) Discovery of a Direct Ras Inhibitor by Screening a Combinatorial Library of Cell-Permeable Bicyclic Peptides. *ACS Comb. Sci. 18*, 75−85.

(14) Welsch, M. E., Kaplan, A., Chambers, J. M., Stokes, M. E., Bos, P. H., Zask, A., Zhang, Y., Sanchez-Martin, M., Badgley, M. A., Huang, C. S., Tran, T. H., Akkiraju, H., Brown, L. M., Nandakumar, R., Cremers, S., Yang, W. S., Tong, L., Olive, K. P., Ferrando, A., and Stockwell, B. R. (2017) Multivalent Small-Molecule Pan-RAS Inhibitors. *Cell 168*, 878−889.

(15) Shima, F., Yoshikawa, Y., Ye, M., Araki, M., Matsumoto, S., Liao, J., Hu, L., Sugimoto, T., Ijiri, Y., Takeda, A., Nishiyama, Y., Sato, C., Muraoka, S., Tamura, A., Osoda, T., Tsuda, K.-i., Miyakawa, T., Fukunishi, H., Shimada, J., Kumasaka, T., Yamamoto, M., and Kataoka, T. (2013) In silico discovery of small-molecule Ras inhibitors that display antitumor activity by blocking the Ras-effector interaction. *Proc. Natl. Acad. Sci. U. S. A. 110*, 8182−8187.

(16) Zhang, Y., Larraufie, M.-H., Musavi, L., Akkiraju, H., Brown, L. M., and Stockwell, B. A.-O. (2018) Design of Small Molecules That Compete with Nucleotide Binding to an Engineered Oncogenic KRAS Allele. *Biochemistry 57*, 1380−1389.

(17) Maurer, T., Garrenton, L. S., Oh, A., Pitts, K., Anderson, D. J., Skelton, N. J., Fauber, B. P., Pan, B., Malek, S., Stokoe, D., Ludlam, M. J., Bowman, K. K., Wu, J., Giannetti, A. M., Starovasnik, M. A., Mellman, I., Jackson, P. K., Rudolph, J., Wang, W., and Fang, G. (2012) Small-molecule ligands bind to a distinct pocket in Ras and inhibit SOS-mediated nucleotide exchange activity. *Proc. Natl. Acad. Sci. U. S. A. 109*, 5299−5304.

(18) Burns, M. C., Sun, Q., Daniels, R. N., Camper, D., Kennedy, J. P., Phan, J., Olejniczak, E. T., Lee, T., Waterson, A. G., Rossanese, O. W., and Fesik, S. W. (2014) Approach for targeting Ras with small molecules that activate SOS-mediated nucleotide exchange. *Proc. Natl. Acad. Sci. U. S. A. 111*, 3401−3406.

(19) Spencer-Smith, R., Koide, A., Zhou, Y., Eguchi, R. R., Sha, F., Gajwani, P., Santana, D., Gupta, A., Jacobs, M., Herrero-Garcia, E., Cobbert, J., Lavoie, H., Smith, M., Rajakulendran, T., Dowdell, E., Okur, M. N., Dementieva, I., Sicheri, F., Therrien, M., Hancock, J. F., Ikura, M., Koide, S., and O'Bryan, J. P. (2017) Inhibition of RAS function through targeting an allosteric regulatory site. *Nat. Chem. Biol. 13*, 62−68.

(20) Rosnizeck, I. C., Graf, T., Spoerner, M., Trankle, J., Filchtinski, D., Herrmann, C., Gremer, L., Vetter, I. R., Wittinghofer, A., Konig, B., and Kalbitzer, H. R. (2010) Stabilizing a weak binding state for effectors in the human ras protein by cyclen complexes. *Angew. Chem., Int. Ed. 49*, 3830−3833.

(21) Halgren, T. (2007) New method for fast and accurate binding-site identification and analysis. *Chem. Biol. Drug Des. 69*, 146−148.

(22) Halgren, T. A. (2009) Identifying and characterizing binding sites and assessing druggability. *J. Chem. Inf. Model. 49*, 377−389.

(23) Lexa, K. W., Goh, G. B., and Carlson, H. A. (2014) Parameter Choice Matters: Validating Probe Parameters for Use in Mixed-Solvent Simulations. *J. Chem. Inf. Model. 54*, 2190−2199.

(24) Ghanakota, P., and Carlson, H. A. (2016) Moving Beyond Active-Site Detection: MixMD Applied to Allosteric Systems. *J. Phys. Chem. B 120*, 8685−8695.

(25) Friesner, R. A., Banks, J. L., Murphy, R. B., Halgren, T. A., Klicic, J. J., Mainz, D. T., Repasky, M. P., Knoll, E. H., Shelley, M., Perry, J. K., Shaw, D. E., Francis, P., and Shenkin, P. S. (2004) Glide: a new approach for rapid, accurate docking and scoring. 1. Method and assessment of docking accuracy. *J. Med. Chem. 47*, 1739−1749.

(26) Young, T., Abel, R., Kim, B., Berne, B. J., and Friesner, R. A. (2007) Motifs for molecular recognition exploiting hydrophobic

DOI: 10.1021/acs.biochem.8b01300
Biochemistry XXXX, XXX, XXX−XXX

enclosure in protein-ligand binding. *Proc. Natl. Acad. Sci. U. S. A. 104*, 808−813.
(27) Abel, R., Young, T., Farid, R., Berne, B. J., and Friesner, R. A. (2008) Role of the active-site solvent in the thermodynamics of factor Xa ligand binding. *J. Am. Chem. Soc. 130*, 2817−2831.
(28) Dixon, A. S., Schwinn, M. K., Hall, M. P., Zimmerman, K., Otto, P., Lubben, T. H., Butler, B. L., Binkowski, B. F., Machleidt, T., Kirkland, T. A., Wood, M. G., Eggers, C. T., Encell, L. P., and Wood, K. V. (2016) NanoLuc Complementation Reporter Optimized for Accurate Measurement of Protein Interactions in Cells. *ACS Chem. Biol. 11*, 400−408.
(29) Lu, S., Jang, H., Nussinov, R., and Zhang, J. (2016) The Structural Basis of Oncogenic Mutations G12, G13 and Q61 in Small GTPase K-Ras4B. *Sci. Rep. 6*, 21949.
(30) Wittinghofer, A. (2014) *Ras superfamily small G proteins: biology and mechanisms*, Springer, New York.
(31) Geyer, M., Schweins, T., Herrmann, C., Prisner, T., Wittinghofer, A., and Kalbitzer, H. R. (1996) Conformational transitions in p21ras and in its complexes with the effector protein Raf-RBD and the GTPase activating protein GAP. *Biochemistry 35*, 10308−10320.
(32) Spoerner, M., Nuehs, A., Ganser, P., Herrmann, C., Wittinghofer, A., and Kalbitzer, H. R. (2005) Conformational states of ras complexed with the GTP analogue GppNHp or GppCH(2)p: Implications for the interaction with effector proteins. *Biochemistry 44*, 2225−2236.
(33) Parker, J. A., Volmar, A. Y., Pavlopoulos, S., and Mattos, C. (2018) K-Ras Populates Conformational States Differently from Its Isoform H-Ras and Oncogenic Mutant K-RasG12D. *Structure 26*, 810.

DOI: 10.1021/acs.biochem.8b01300
Biochemistry XXXX, XXX, XXX−XXX